

Electrical and dielectric properties of Nd-doped SrBi₂Ta₂O₉ ceramics

Mohamed Afqir^{1,*}, Yingzhi Meng², Didier Fasquelle³, Amina Tachafine³, Mohamed Daoud¹, Mohamed Elahtmani

¹*Cadi Ayyad University, Faculty of Sciences, Physical Chemistry of Materials and the Environment, Marrakesh, Morocco*

²*Guilin University of Technology, Guilin 541006, China*

³*University of Littoral-Côte d'Opale, Dynamics and Structure of Molecular Materials Unit, Calais, France*

Received 17 February 2025; received in revised form 29 May 2025; accepted 11 June 2025

Abstract

Combination of molten-salt and calcination techniques was used to synthesize Nd-doped SrBi₂Ta₂O₉ ($x = 0, 0.02, 0.05$ and 0.1) ceramic powders. The prepared powders were uniaxially pressed and sintered at 1200 °C for 6 h. The suggested approach allows obtaining pure products without secondary phases, while the Nd content slightly affected the unit cell parameters. The diffusivity of the dielectric maximum increases and the Curie temperature decreases with the increase of Nd concentration. The non-overlapping small polaron tunneling remained the predominant conduction process. Within the temperature range from 300 to 450 °C, both the bulk grain and the grain boundary resistances were determined from the Nyquist plots. It was shown that the grain boundary resistivity decreases with temperature owing to the charge carriers' movement and the grain boundary and grain resistivities decrease when Nd was introduced in the SrBi₂Ta₂O₉ structure.

Keywords: SrBi₂Ta₂O₉, Nd-doping, molten salt, dielectric, electrical conductivity

I. Introduction

Aurivillius compounds can be categorized into one of four different types, i.e. bismuth layered-structured ferroelectrics (BLSFs), bismuth metal vanadium oxide (BIMEVOX), halide and bismuth-layered composites [1–3]. The Aurivillius-type layered ferroelectrics (BLSFs) have found extensive use in optical, piezoelectric, non-volatile ferroelectric and transducer applications as well as capacitors and transducers [4]. Sillén-Aurivillius-type oxyhalide compounds are suitable for semiconductors [1], whereas the Aurivillius-type composites exhibit good ferroelectric, piezoelectric, multiferroic and magnetoelectric properties. On the other hand, the Aurivillius-type conducting oxides (BIMEVOX) are components for oxide-ion electrolytes in solid oxide fuel cells (SOFCs).

SrBi₂Ta₂O₉ belongs to the Aurivillius family of bismuth layer-structured ferroelectric materials, which are the main candidate materials for producing non-volatile memory chips [4–6]. Recently, there have been tremendous numbers of studies that investigate

the photocatalytic CO₂ reaction [21]. Frustrated Lewis pairs (FLP) were fabricated on SrBi₂Ta₂O₉ for photocatalytic reduction of CO₂. FLP-fractionalized oxygen vacancies in SrBi₂Ta₂O₉-hydroxyl compound show an excellent CO₂ reduction performance compared to that of SrBi₂Ta₂O₉. Furthermore, what specifically characterizes the double-layer Aurivillius phase is high Curie temperature, excellent polarization fatigue-free behaviour, fast switching and low leakage currents. However, these compounds suffer from low polarization arising from a low dielectric constant and high dielectric loss. Therefore, lead zirconate titanate (PZT) has shown better piezoelectric behaviour compared to the Aurivillius-type layered ferroelectric materials. Ferroelectric properties can be improved by adjusting the partial substitution and optimal sintering temperature. In this regard, isovalent dopants, which are of similar valence to bismuth, lower the Curie point, enhance the dielectric constant and lower the dielectric loss. It is commonly discussed that for small concentrations of neodymium in BLSF ceramics, the remnant polarization ($2P_r$) can reach the maximum value and the coercive field (E_c) may remain almost unchanged. Also, when Nd doping exceeds certain levels, the compounds exhibit relaxation behaviour [22,23]. The cited studies may have already

*Corresponding author: tel: + 212 701231987
e-mail: mohamed.afqir@yahoo.fr

investigated the role of Nd in the $\text{SrBi}_2\text{Ta}_2\text{O}_9$ structure, while the role of this dopant on electrical properties had not yet been investigated.

There are many publications related to $\text{SrBi}_2\text{Ta}_2\text{O}_9$ materials, but the synthesis of desirable $\text{SrBi}_2\text{Ta}_2\text{O}_9$ powders still needs to be optimized. In addition, the efficient sintering process for enhancing dielectric properties has been questionably tailored and desirable enhanced spontaneous polarization may be difficult to achieve.

Based on our previous paper [2], the presented work consists of two parts. In the first, fabrication of $\text{SrBi}_{2-x}\text{Nd}_x\text{Ta}_2\text{O}_9$ ($x = 0, 0.02, 0.05, \text{ and } 0.1$) ceramic compounds, as well as their structural characterization were presented. The second part highlights dielectric measurements combined with a theoretical approach.

II. Experimental

The molten salt method was used to synthesize the $\text{SrBi}_{2-x}\text{Nd}_x\text{Ta}_2\text{O}_9$ ($x = 0, 0.02, 0.05, \text{ and } 0.1$) samples. In the first step, Bi_2O_3 (Rectapur 90%), Ta_2O_5 , Nd_2O_3 (HiMedia 99.9%) and SrCO_3 (Fluka 98%) were ground in stoichiometric proportions. Then, these precursors were stirred in a $\text{NaNO}_3\text{-KNO}_3$ mixture at 400°C for 3 h. After that, the process of filtration was carried out to separate an insoluble component from the soluble $\text{NaNO}_3\text{-KNO}_3$ mixture using diluted acid as a solvent. The obtained powder mixtures were milled manually and then calcined at 1000°C for 8 h. The calcined powders were uniaxially pressed into pellets (under 2 t/m^2) and then sintered at temperatures of 1200°C in air for 6 h. The ceramics were coated on both sides with silver paste to enable electrical and dielectric measurements.

Phase composition and purity of the prepared material were determined by X-ray diffraction (Bruker D8) with $\text{CuK}\alpha$ ($\lambda = 1.5406\text{ \AA}$) radiation in the range $5^\circ < 2\theta < 70^\circ$ at a scanning rate of $5^\circ/\text{min}$. Unit cell and lattice parameters were computed using UnitCell and HighScore Plus programs. The Archimedes technique and XRD data were used to measure and calculate the experimental and theoretical densities.

The Agilent 4284A was used to test the dielectric and electrical properties as a function of frequency and temperature.

III. Results and discussion

3.1. Structural characterization

Figure 1 displays the XRD spectra of the sintered samples. The $\text{SrBi}_2\text{Ta}_2\text{O}_9$ (JSPDS NO. 49-0609) standard pattern fits all of the sample diffraction peaks, indicating the effective synthesis of $\text{SrBi}_{2-x}\text{Nd}_x\text{Ta}_2\text{O}_9$ ($x = 0, 0.02, 0.05$ and 0.1) compounds without any secondary phase. In addition, the diffraction intensities do not show any preferred orientations.

Figure 2 illustrates changes in lattice parameters as a function of Nd content in the $\text{SrBi}_{2-x}\text{Nd}_x\text{Ta}_2\text{O}_9$ compounds. Changes in the lattice parameters, a , b and c , are associated with a shift in the XRD peaks caused by Nd doping. The a , b and c values, together with the unit cell volume, decrease when the amount of Nd increases in $\text{SrBi}_2\text{Ta}_2\text{O}_9$. However, these lattice parameters and amount x do not exhibit a linearly dependent relationship (Fig. 2). The changes in lattice parameters may not only be attributed to the incorporation of Nd^{3+} (0.983 \AA [7]) in the Bi^{3+} site (1.03 \AA [7]), but also can be attributed to the measurement accuracy.

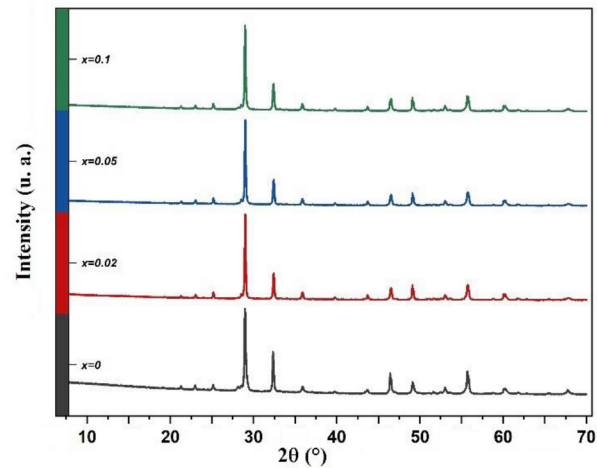


Figure 1. XRD spectra of $\text{SrBi}_{2-x}\text{Nd}_x\text{Ta}_2\text{O}_9$ ($x = 0, 0.02, 0.05$ and 0.1) compounds

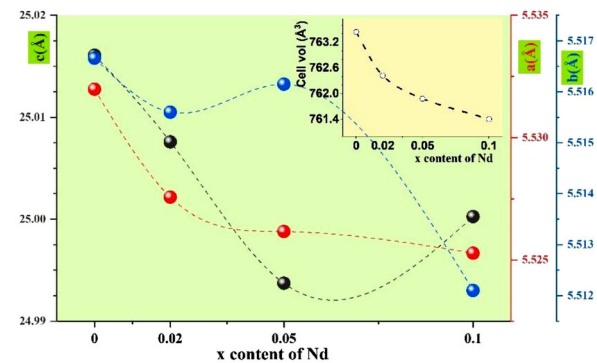


Figure 2. Variation of lattice parameters (a , b and c) and volume of the unit cell for $\text{SrBi}_{2-x}\text{Nd}_x\text{Ta}_2\text{O}_9$ ($x = 0, 0.02, 0.05$ and 0.1) compounds

In spite of different experimental processes for pellet preparation, such as use of different type of binder, uniaxial pressure and ball mill conditions, most

of the experimental studies showed significant changes in density because of sintering temperature [8,9]. Consequently, when pellets were sintered at 1200 °C, their densities achieved the maximum value. On the other hand, when the compounds were sintered at temperatures above 1200 °C, decomposition of bulk ceramics occurred and SrTa₂O₆ phase was formed,

which could coexist with SrBi₂Ta₂O₉ [10–13]. In this sense, this work evidences that 1200 °C/6h remains the optimal condition, allowing not only to get a relative density of 88–92 %TD (percentage of theoretical density), but also to avoid the decomposition process. Meanwhile the Nd content did not bring significant change on densit.

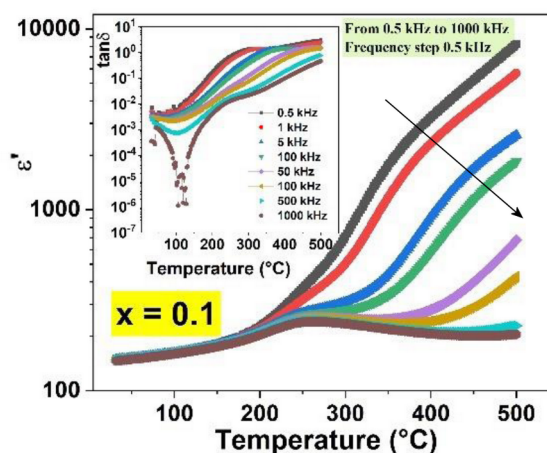
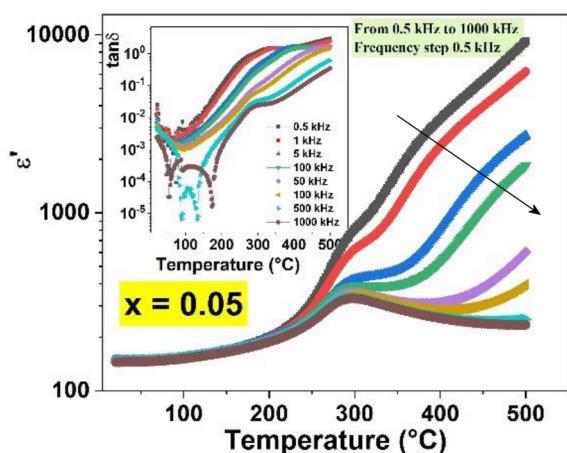
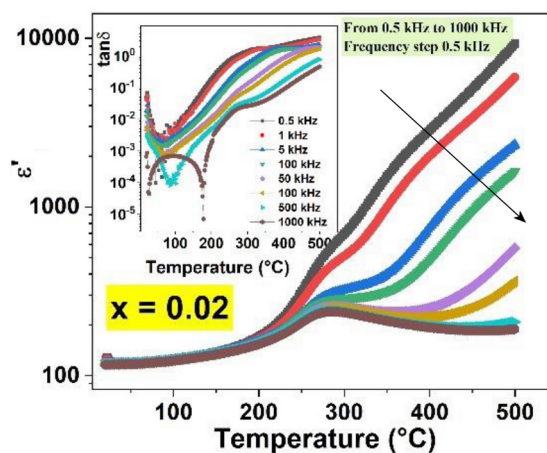
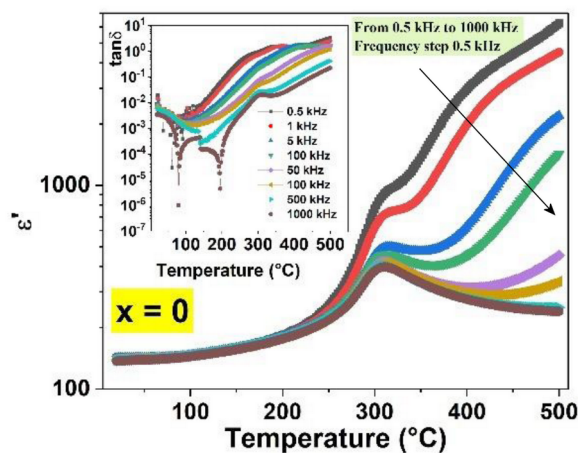


Figure 3. Temperature and frequency dependence of dielectric constant (ϵ') and dielectric loss ($\tan\delta$, inset) of SrBi_{2-x}Nd_xTa₂O₉ ceramics: a) $x = 0$, b) $x = 0.02$, c) $x = 0.05$ and d) $x = 0.1$

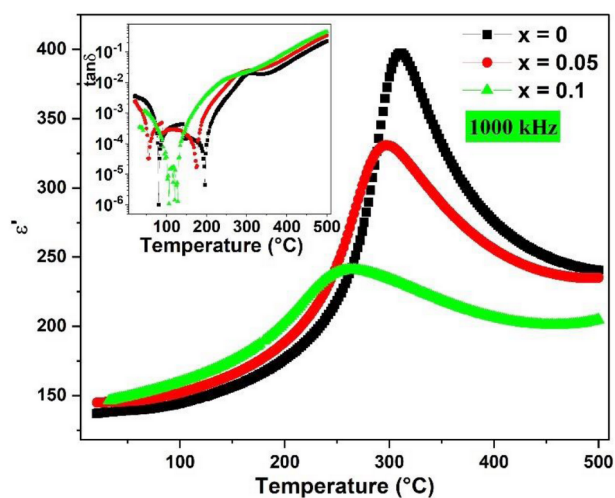


Figure 4. Temperature dependence of dielectric constant (ϵ') and dielectric loss ($\tan\delta$, inset) of SrBi_{2-x}Nd_xTa₂O₉ ($x = 0, 0.05$ and 0.1) ceramics measured at 1 MHz

3.2. Dielectric properties

Frequency dependence of dielectric constant and dielectric loss curves, measured as a function of temperature, are shown in Fig. 3. Overall, as one goes to high temperature, it can be seen that all ϵ' -curves exhibit a maximum (ϵ'_{max}) referring to the Curie temperature and transition from ferroelectric to paraelectric phase. The Curie temperature (T_C) of the dopant-free SrBi₂Ta₂O₉ sample is 316 °C, which is similar as in the literature [2,14]. The dielectric constant curve for the pure SrBi₂Ta₂O₉ (Fig. 3) is similar to that published elsewhere [2]. However, the only difference is the maximal dielectric constant at

the Curie temperature, i.e. it is ~500 in this work and ~1600 in our previous paper [2]. This difference may be attributed to the different sintering conditions, but also due to the different ceramic pellet dimension.

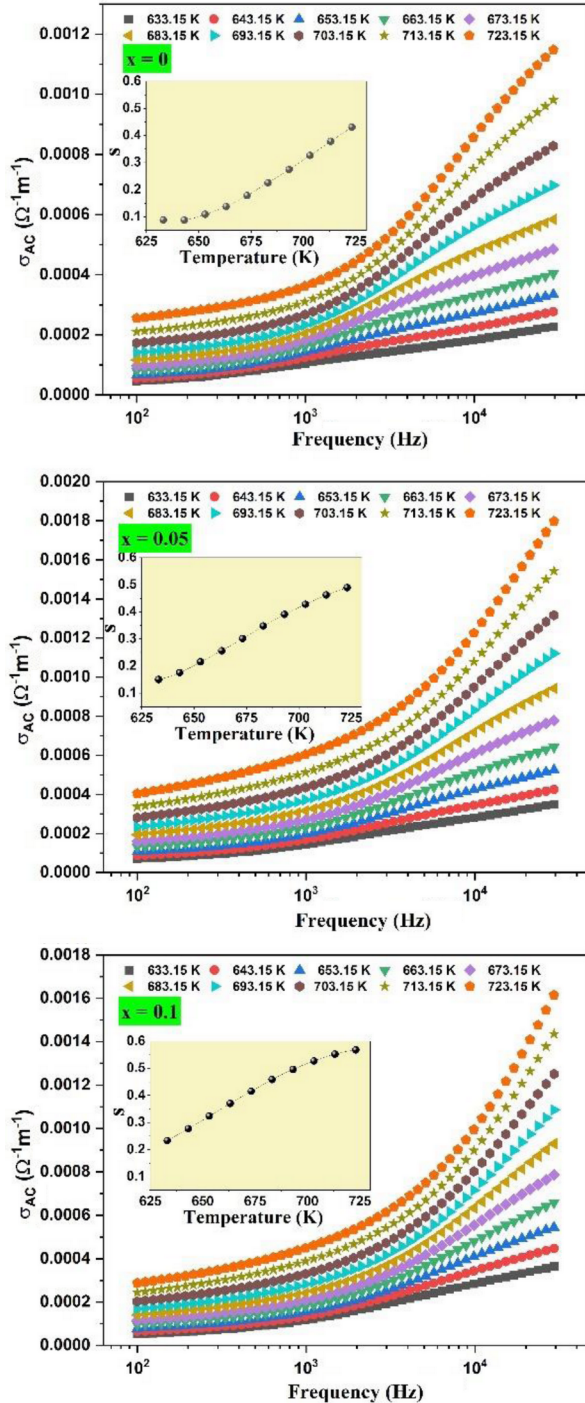


Figure 5. Variation of electrical conductivity as a function of frequency and temperature of SrBi_{2-x}Nd_xTa₂O₉ ceramics: a) $x = 0$, b) $x = 0.05$ and c) $x = 0.1$

Influence of Nd concentration on the dielectric constant (ϵ') and dielectric loss ($\tan\delta$) can be clearly seen in Fig. 4. From room temperature until $<200^\circ\text{C}$, the $x = 0.1$ sample has the highest dielectric constant

when compared to other samples. However, ϵ'_{max} is around 400, 330 and 244 for the SrBi_{2-x}Nd_xTa₂O₉ ceramics having $x = 0, 0.05$ and 0.1 , respectively. The fact that the peaks (ϵ'_{max}) are independent of frequency (Fig. 3) confirms that the samples have normal ferroelectric behaviour. In addition, it is obvious that an increase in Nd concentration leads to a decrease in the Curie temperature (Fig. 3), which adheres to the traditional experiments where transition temperature tends to decrease with the increase of rare earth content [15]. Thus, the T_C shift to a lower temperature may be advantageous for achieving a high dielectric constant near room temperature.

Regarding dielectric loss ($\tan\delta$), it is almost the same for all samples at 1 MHz. When all polarization processes are activated within materials, the dielectric loss ($\tan\delta$) experiences a decrease, mainly below 200°C .

The modified Curie-Weiss law can be used to calculate the degree of diffusion [14,16]. Thus, it is clear from Fig. 4 that the diffusion of the dielectric maximum increases as the amount of neodymium increases.

3.3. Conductivity

The AC conductivity (σ_{AC}) curves of the prepared samples, given in Fig. 5, are fitted by the Jonscher's universal power law:

$$\sigma_{AC} = \sigma_{DC} + A\omega^s \quad (1)$$

$$\omega = 2\pi \cdot f \quad (2)$$

where σ_{DC} , f , A and s are DC conductivity, frequency, temperature-dependent constant and an exponent, respectively. There are two distinct regions in Fig. 5. The first part, where conductivity is frequency-independent, is found at low frequencies. In the second region, which could be fitted by hopping between charge carriers, the increase of conductivity is not only frequency dependent, but also increases with temperature. According to Fig. 5, the temperature dependence of the exponent s indicates that, primarily for the doped samples, non-overlapping small polaron tunnelling (NSPT) [17] is the predominant conduction process in the specified temperature range.

The Nyquist plots for the prepared samples at different temperatures are illustrated in Fig. 6. Overall, resistivities of grain boundaries and grains are responsible for the large arc seen at low frequencies and the small arc at high frequencies, respectively. Each arc is described by a parallel RQ circuit, where R and Q represent the resistance and the constant phase element, respectively. The grain boundary resistivity shows strong dependence on the temperature, whereas the grain resistivity dependence on temperature is not obvious. The Nyquist plots bring out two essential points. The first, the grain boundary resistivity decreases with temperature owing to the charge

carriers' movement. The second, when Nd was introduced in the $\text{SrBi}_2\text{Ta}_2\text{O}_9$ structure, the grain boundary and grain resistivities decrease. In general, increased Nd addition leads to increased conductivity due to the higher concentration of carriers.

Electrical impedance (Z) and dielectric loss ($\tan\delta$) versus frequency (log-log scale) at selected temperatures are given in Fig. 7. Overall, the electrical impedance decreases with increasing temperature and frequency that exhibited the capacitive characteristic. However, $\tan\delta$ increases with temperature while decreases with frequency arising from delay of polarization in the ceramics. As a result, the samples

witness the influence of the intrinsic dielectric properties. At the low-frequency region, from 10^2 to 10^3 Hz, the charge carrier mobility is impeded not only by grain boundaries, but also by the existence of defects and oxygen vacancies, which may trap this motion. At a higher frequency ($>10^3$ Hz), the charge carriers do not require more energy to move freely through the grain boundaries. Meanwhile, the electrical circuit, used in the Nyquist plots (Fig. 6), confirms that the sample has lower resistance at higher temperatures. Thus, the higher the capacitance (C), the lower the impedance ($1/|Z| = 2fC$).

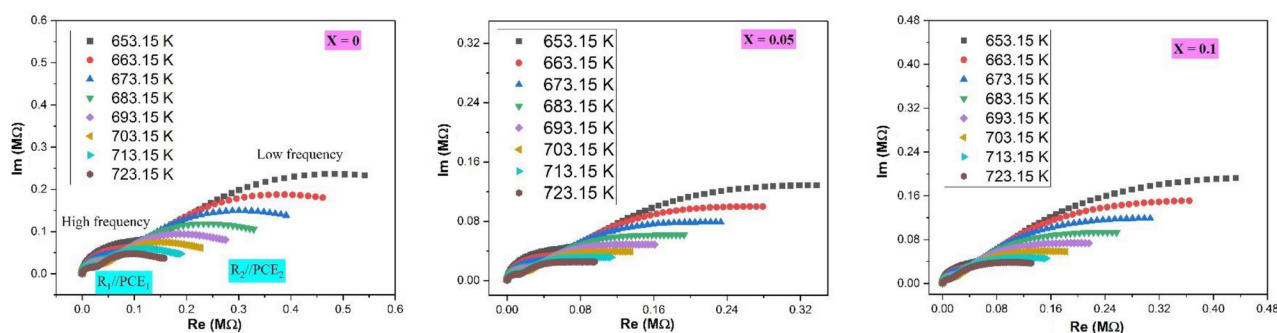


Figure 6. The Nyquist plots for $\text{SrBi}_{2-x}\text{Nd}_x\text{Ta}_2\text{O}_9$ ceramics: a) $x = 0$, b) $x = 0.02$, c) $x = 0.05$ and d) $x = 0.1$

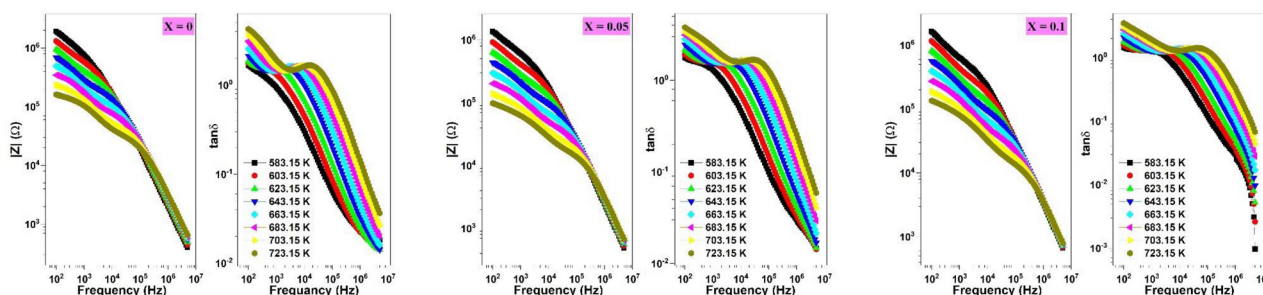


Figure 7. Normalized imaginary component of impedance against frequency for $\text{SrBi}_{2-x}\text{Nd}_x\text{Ta}_2\text{O}_9$ ($x = 0, 0.05$ and 0.1) ceramics

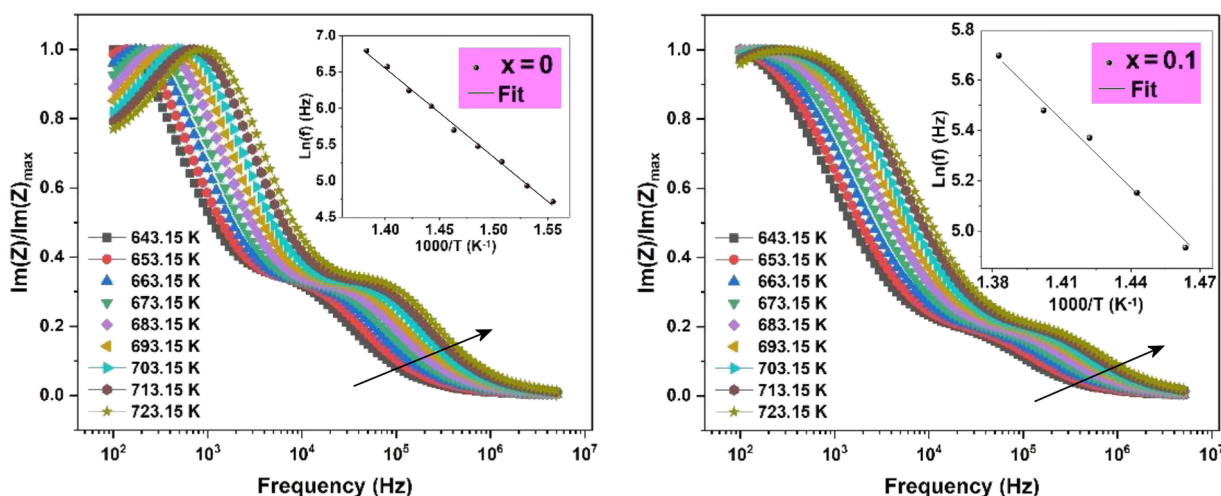


Figure 8. Impedance against frequency and temperature for $\text{SrBi}_{2-x}\text{Nd}_x\text{Ta}_2\text{O}_9$ ($x = 0$ and 0.1) ceramics

In Fig. 8, the normalized imaginary component of impedance is plotted against frequency. The samples, mainly the undoped sample, exhibit peaks that shift towards high frequency. The relaxation activation energy (E_a) is obtained from the fit of Eq. 3 after linearization:

$$f = f_0 \cdot e^{\frac{-E_a}{k_B T}} \quad (3)$$

where f , f_0 , and k_B are the peak frequency, pre-exponential factor and the Boltzmann constant, respectively. The undoped sample has the highest ($E_a = 2.4$ eV), whereas the $\text{SrBi}_{1.9}\text{Nd}_{0.1}\text{Ta}_2\text{O}_9$ sample has the lowest relaxation activation energy ($E_a = 1.8$ eV). As a result, the charge carriers find it more difficult to pass through the grain boundary when the relaxation activation energy is higher [10]. This activation energy might be relatively high, suggesting the domination of oxygen ion vacancies arising from sintering at high temperature.

Overall, the ceramic samples annealing in air leads to the formation of oxygen vacancies, which remain the key factor in varying either dielectric loss or electrical conductivity. At high temperatures, 300 °C–450 °C, the effects of Nd on the electrical properties of $\text{SrBi}_2\text{Ta}_2\text{O}_9$ ceramics could not be accurately determined through electrical approaches. There are tremendous factors that alter electrical results. The coupling of point defects forms an electron-pinned defect-dipoles (EPDD) effect and induces strong hopping polarization. In addition, an internal barrier layer capacitance (IBLC) effect and a surface barrier layer capacitor (SBLC) effect [18–20] may outweigh the Nd effect. In this case, it might be because there was not much Nd in the $\text{SrBi}_2\text{Ta}_2\text{O}_9$ structure. The mechanisms mentioned above, EPDD, IBLC and SBLC, hamper expression of the Nd effects above the Curie temperature

IV. Conclusions

The molten salt technique was used to fabricate $\text{SrBi}_{2-x}\text{Nd}_x\text{Ta}_2\text{O}_9$ ($x = 0, 0.02, 0.05$ and 0.1) ceramics. The compounds were highly pure when they were calcined at 1000 °C and sintered at 1200 °C. It was observed that when the Nd content increased, the unit cell slightly shrunk. The selected optimal sintering conditions at 1200 °C for 6 h allowed fabrication of the Nd-doped $\text{SrBi}_2\text{Ta}_2\text{O}_9$ ceramics with relative density of 88–92 %TD.

The Curie temperature of the dopant-free $\text{SrBi}_2\text{Ta}_2\text{O}_9$ sample is 316 °C and it decreases with the increase in Nd concentration. It is also obvious that the diffusivity of the dielectric maximum increases with Nd content. Electrical and dielectric measurements (from 300 to 450 °C) revealed that the grain boundary resistivity decreases with temperature owing to the

charge carriers' movement by non-overlapping small polaron tunnelling.

References

1. D. Ozaki, H. Suzuki, O. Tomita, Y. Inaguma, K. Nakashima, H. Kageyama, R. Abe, "A new lead-free Sillén-Aurivillius oxychloride $\text{Bi}_5\text{SrTi}_3\text{O}_{14}\text{Cl}$ with triple-perovskite layers for photocatalytic water splitting under visible light", *J. Photochem. Photobiol. A Chem.*, **408** (2021) 113095.
2. M. Afqir, D. Fasquelle, A. Tachafine, M. Elaamrani, Y. Meng, M. Daoud, "Effects of La doping on diffused ferroelectric phase transition, electric and dielectric properties of lead-free $\text{SrBi}_2\text{Ta}_2\text{O}_9$ ceramics", *Process. Appl. Ceram.*, **18** [3] (2024) 290–298.
3. S. Khasa, P. Singh, S. Sanghi, N. Singh, A. Agarwal, "Science and technology structural analysis and dielectric characterization of Aurivillius type $\text{CaSrBi}_2\text{Nb}_2\text{O}_9$ ceramics", *J. Integr. Sci. Technol.*, **2** [1] (2014) 13–21.
4. S.K. Rathaur, R. Khosla, S.K. Sharma, "Metal (Pt)/ferroelectric ($\text{SrBi}_2\text{Ta}_2\text{O}_9$)/insulator (La_2O_3)/semiconductor (Si), MFIS structures for nonvolatile memory applications", *Appl. Phys. Lett.*, **119** (2021) 063505.
5. A. Hartmann, R. Lamb, J. Scott, C. Gutleben, "The bandgap of $\text{SrBi}_2\text{Ta}_2\text{O}_9$ ", *Integ. Ferroelectrics*, **18** (1997) 101–108.
6. K. Watanabe, A.J. Hartmann, R.N. Lamb, R.P. Craig, S.M. Thurgate, J.F. Scott, "Valence band and bandgap states of ferroelectric $\text{SrBi}_2\text{Ta}_2\text{O}_9$ thin films", *Jpn. J. Appl. Phys.*, **39** (2000) L309.
7. R.D. Shannon, "Revised effective ionic radii and systematic studies of interatomic distances in halides and chalcogenides", *Acta Crystallogr. Sect. A*, **32** [5] (1976) 751–767.
8. A. Rashid, M. Ikram, "Effect of sintering temperature on the structural, morphological, optical, magnetic, and dielectric properties of lead free $\text{La}_2\text{SrFe}_{1.7}\text{Ni}_{0.3}\text{TiO}_9$ triple perovskite", *J. Mater. Sci. Mater. Electron.*, **36** (2025) 206.
9. A. Castro, P. Millán, L. Pardo, B. Jiménez, "Synthesis and sintering improvement of Aurivillius type structure ferroelectric ceramics by mechanochemical activation", *J. Mater. Chem.*, **9** (1999) 1313–1317.
10. B. Li, L. Li, X. Wang, "Sintering behavior of bulk $\text{SrBi}_2\text{Ta}_2\text{O}_9$ prepared by solid-state reaction", *Ceram. Int.*, **29** (2003) 351–353.
11. C.H. Lu, Y.C. Chen, "Sintering and decomposition of ferroelectric layered perovskites: Strontium bismuth tantalate ceramics", *J. Eur. Ceram. Soc.*, **19** [16] (1999) 2909–2915.
12. B. Li, X. Wang, X. Han, X. Qi, L. Li, "Spark-plasma-sintering of bulk $\text{SrBi}_2\text{Ta}_2\text{O}_9$ materials", *J. Mater. Sci.*, **39** (2004) 2621–2623.
13. C.H. Lu, Y.H. Huang, "Densification and dielectric properties of strontium bismuth tantalate ceramics", *Adv. Appl. Ceram.*, **107** [6] (2008) 305–309.
14. V. Senthil, T. Badapanda, A. Chandrabose, S. Panigrahi, "Dielectric and ferroelectric behavior of

- cerium modified SrBi₂Ta₂O₉ ceramic”, *Mater. Lett.*, **159** (2015) 138–141.
15. M. Afqir, A. Tachafine, D. Fasquelle, M. Elaammani, J.C. Carru, A. Zegzouti, M. Daoud, “Dielectric properties of SrBi_{1.8}RE_{0.2}Nb₂O₉ (RE = Yb, Tm, Tb, Gd, Er, Sm and Ce) ceramics”, *Solid State Sci.*, **73** (2017) 51–56.
 16. Z. Wang, Y. Meng, S. Tang, X. Niu, H. Zhang, D. Wang, Y. Bai, B. Peng, X. Chen, Q. Ke, S.-G. Lu, L. Liu, “Simultaneous achievement of large electrocaloric effect and ultra-wide operating temperature range in BaTiO₃-based lead-free ceramic”, *J. Adv. Ceram.*, **13** [8] (2024) 1234–1241.
 17. M. Jebli, C. Rayssi, J. Dhahri, M. Ben Henda, H. Belmabrouk, A. Bajahzar, “Structural and morphological studies, and temperature/frequency dependence of electrical conductivity of Ba_{0.97}La_{0.02}Ti_{1-x}Nb_{4x/5}O₃ perovskite ceramics”, *RSC Adv.*, **11** [38] (2021) 23664–23678.
 18. L. Wang, J. Li, X. Liu, M. Zhang, X. Li, S. Liu, X. Sun, “Effect of different defects on the polarization mechanism of (Nb,Ga) codoped TiO₂ single crystals”, *Ceram. Int.*, **49** [19] (2023) 32116–32126.
 19. I. Norezan, A. K. Yahya, M. K. Talari, “Effect of (Ba_{0.6}Sr_{0.4})TiO₃ (BST) doping on dielectric properties of CaCu₃Ti₄O₁₂ (CCTO)”, *J. Mater. Sci. Technol.*, **28** [12] (2012) 1137–1144.
 20. Y. Meng, K. Liu, X. Zhang, X. Lei, J. Chen, Z. Yang, B. Peng, C. Long, L. Liu, C. Li, “Defect engineering in rare-earth-doped BaTiO₃ ceramics: Route to high-temperature stability of colossal permittivity”, *J. Am. Ceram. Soc.*, **105** [9] (2022) 5725–5737.
 21. K. Wang, Y. Du, Y. Li, X. Wu, H. Hu, G. Wang, Y. Xiao, S. Chou, G. Zhang, “Atomic-level insight of sulfidation-engineered Aurivillius-related Bi₂O₂SiO₃ nanosheets enabling visible light low-concentration CO₂ conversion”, *Carbon Energy*, **5** [2] (2023) 1–11.
 22. S.A. Ivanov, T. Sarkar E.A. Fortalnova, E.D. Politova, S.Y. Stefanovich, M.G. Safronenko, P. Nordblad, R. Mathieu, “Composition dependence of the multifunctional properties of Nd-doped Bi₄Ti₃O₁₂ ceramics”, *J. Mater. Sci. Mater. Electron.*, **28** [11] (2017) 7692–7707.
 23. H. Zhang, H. Yan, M.J. Reece, “The effect of Nd substitution on the electrical properties of Bi₃NbTiO₉ Aurivillius phase ceramics”, *J. Appl. Phys.*, **106** [4] (2009) 44106.